



1 **Significant contribution of HONO to secondary**
2 **pollutants during a severe winter pollution event in**
3 **southern China**

4 **Xiao Fu**^a, **Tao Wang**^{a,*}, **Li Zhang**^{a,b}, **Qinyi Li**^{a,**}, **Zhe Wang**^a, **Men Xia**^a, **Hui Yun**^a,
5 **Weihao Wang**^a, **Chuan Yu**^a, **Dingli Yue**^c, **Yan Zhou**^c, **Junyun Zheng**^d, **Rui Han**^e

6 ^a Department of Civil and Environmental Engineering, Hong Kong Polytechnic University,
7 Hong Kong 99907, China

8 ^b Atmospheric and Oceanic Sciences, Princeton University, Princeton, New Jersey 08540,
9 United States

10 ^c Guangdong Provincial Environmental Monitoring Center, Guangzhou, China

11 ^d Institute for Environmental and Climate Research, Jinan University, Guangzhou, China

12 ^e National Meteorological Information Center, China Meteorological Administration, Beijing
13 100081, China

14 * *Correspondence to:* Tao Wang (tao.wang@polyu.edu.hk)

15 ** Now at: Department of Atmospheric Chemistry and Climate, Institute of Physical Chemistry
16 Rocasolano, CSIC, Madrid 28006, Spain

17

18 **Abstract**

19 Nitrous acid (HONO) can strongly affect atmospheric photochemistry in polluted
20 regions through the production of hydroxyl radical (OH). In January 2017, a severe pollution
21 episode occurred in the Pearl River Delta (PRD) of China, with maximum hourly PM_{2.5},
22 ozone and HONO levels reaching 400 µg/m³, 150 ppb, and 8 ppb, respectively, at a suburban
23 site. The present study investigated the sources/processes generating such high HONO
24 concentrations and the role of HONO chemistry in this severe winter episode. Four recently
25 reported HONO sources were added to the Community Multi-scale Air Quality (CMAQ)
26 model, including RH-dependent and light-enhancing effects on heterogeneous reactions,
27 photolysis of particulate nitrate in the atmosphere, and photolysis of HNO₃ and nitrate on
28 surfaces. The revised model reproduced the observed HONO and significantly improved its
29 performance for O₃ and PM_{2.5}. The model simulations showed that the heterogeneous
30 generation on surfaces (with RH and light effects) was the largest contributor (72%) to the
31 predicted HONO concentrations, with the RH-enhancing effects more significant at nighttime
32 and the light-enhancing effects more important in the daytime. The photolysis of total nitrate
33 in the atmosphere and deposited on surfaces was the dominant HONO source during noon and
34 afternoon, contributing above 50% of the simulated HONO. The HONO photolysis was the
35 dominant contributor to HO_x production in this episode. With all HONO sources, the daytime
36 average O₃ at Heshan site was increased by 24 ppb (or 70%), compared to the simulation
37 results without any HONO sources. Moreover, the simulated mean concentrations of TNO₃
38 (HNO₃ + fine particle NO₃⁻) at Heshan site, which was the key species for this haze formation,
39 increased by about 17 µg/m³ (67%) due to the HONO chemistry, and the peak enhancement
40 reached 55 µg/m³. This study highlights the key role of HONO chemistry in the formation of
41 winter haze in a subtropical environment.

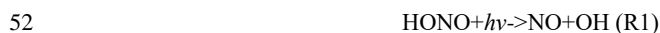
42

43



44 1 Introduction

45 Nitrous acid (HONO) can significantly affect atmospheric photochemistry through its
46 photolysis producing hydroxyl radical (OH) (R1) and subsequent reactions of OH with other
47 gases (Alicke et al., 2003; Kleffmann et al., 2005). OH radical oxidizes volatile organic
48 compounds (VOC) and converts nitric oxide (NO) into nitrogen dioxide (NO₂) without
49 consuming ozone (O₃), leading to the generation of O₃ (R2 to R6). The oxidation of oxides of
50 nitrogen (NO_x=NO+NO₂), sulfur dioxide (SO₂) and VOC by OH, O₃ and H₂O₂ also produce
51 secondary aerosols, which are the key components of haze (e.g., Cao et al., 2012).



58 The impact of HONO on atmospheric photochemistry varies under different
59 environmental conditions. In general, the effect of HONO is more significant in polluted
60 conditions than clean conditions. For example, calculations constrained by field
61 measurements of HONO have suggested that the contributions of HONO photolysis to the
62 daytime HO_x (HO_x = OH + HO₂) production can reach 56% in an urban area (Ren et al.,
63 2003) and 87% at a roadside (Yun et al., 2017), which are higher than the contributions in
64 rural and forested areas (30% to 40%) (Acker et al., 2006; Kleffmann et al., 2005).
65 Simulations by chemistry transport model which considered major sources of HONO showed
66 that the maximum enhancements of O₃ concentrations due to HONO were mostly less than 10
67 ppb in the US and other western countries (Sarwar et al., 2008; Czader et al., 2012; Li et al.,
68 2010; Goncalves et al., 2012), but more significant impacts have been reported in China due
69 to more intense NO_x and VOC emissions. For example, the reported maximum hourly O₃
70 enhancement can be more than 30 ppb in Beijing (Li et al., 2011; Xu et al., 2006) and up to 25
71 ppb in Hong Kong (Zhang et al., 2016). The previous studies mostly focused on summertime.
72 Limited attention has been paid to the winter season when the observed HONO



73 concentrations can also be high (Hou et al., 2016; Li et al., 2018a; Wang et al., 2016; Xu et al.,
74 2015).

75 The source and formation mechanism of HONO are still not fully understood. Most
76 previous studies suggest that heterogeneous reaction of NO₂ on surface is dominant,
77 especially at night (Li et al., 2012; Wang et al., 2017a; Zhang et al., 2016). In the daytime, the
78 long-known gas-phase reaction of NO and OH explains less than 10% of the daytime HONO
79 production (Sarwar et al., 2008; Li et al., 2010; Zhang et al., 2016). Other daytime sources
80 include direct traffic emissions (Kurtenbach et al., 2001; Liang et al., 2017), humidity and
81 light-dependent heterogeneous generation (Finlayson-Pitts et al., 2003; Ndour et al., 2008;
82 Monge et al., 2010), soil emissions (Oswald et al., 2013; Su et al., 2011; Meusel et al., 2018),
83 photolysis of particle nitrate in the atmosphere (Ye et al., 2016b, 2017), and photolysis of
84 deposited HNO₃ and nitrate on the ground (Ye et al., 2016a; Zhou et al., 2011), etc.

85 During 4-8 January 2017, a severe winter air pollution event occurred in the Pearl River
86 Delta (PRD), a region long known to suffer from photochemical pollution due to its fast
87 industrialization (Chan and Yao, 2008; Wang et al., 1998, 2003, 2017b; Xue et al., 2014;
88 Zhang et al., 2008; Zheng et al., 2010). During this multi-day episode, an hourly peak value of
89 ~150 ppb for O₃ and ~400 µg/m³ for PM_{2.5} were observed, and the HONO levels reached 8
90 ppb, with an average value of 2.9 ppb at night (18:00 to 6:00) and 2.4ppb in daytime (7:00 to
91 17:00). The HONO values were among the highest ever reported in China (Bernard et al.,
92 2016; Huang et al., 2017; Li et al., 2012; Qin et al., 2009; Su et al., 2008; Wang et al., 2017a;
93 Wang et al., 2013; Li et al., 2018a; Xu et al., 2015). It is of great interest to find out how such a
94 high level of HONO was produced and what impact it had on the radical levels and secondary
95 pollutants during this severe winter pollution event.

96 The present study utilizes the CMAQ model with up-to-date HONO sources, including
97 those in the original CMAQ model (gas-phase generation, heterogeneous reaction, and
98 vehicle emissions) and four newly added sources (RH-enhancing effects on heterogeneous
99 reactions, light-enhancing effects on heterogeneous reactions, photolysis of particulate nitrate
100 in the atmosphere, and photolysis of HNO₃ and nitrate adsorbed on surfaces). The updated
101 model was then used to analyze the contributions of different HONO sources, and also to
102 quantify the contributions of HONO to secondary pollutants during this severe winter



103 pollution event. Our study reveals the very large impact of HONO on winter-time chemistry
104 at this subtropical site.

105 **2 Materials and Methods**

106 **2.1 Model description**

107 **2.1.1 CMAQ model configurations and inputs**

108 CMAQ version 5.1 with the updated carbon bond 2005 e51 (CB05e51) gas mechanism
109 and AERO6 aerosol mechanism (Appel et al., 2017) was used in this study. One-way triple
110 nesting domains were used with their horizontal resolutions being 36, 12, and 4 km,
111 respectively, and the innermost domain covers the PRD region (Fig. 1). These domains are
112 based on a Lambert projection with two true latitudes of 25° N and 40° N. The objective
113 simulation period was 4 to 8 January 2017, with three days before as a spin-up time.

114 The Weather Research & Forecasting Model (WRF) version 3.7 was applied to generate
115 the meteorological fields for the CMAQ simulations. The physical options used in the WRF
116 model were the Lin microphysics scheme (Lin et al., 1983), Rapid Radiative Transfer Model
117 for GCMs (RRTMG) shortwave and longwave radiation scheme (Mlawer and Clough, 1998;
118 Mlawer et al., 1997), Noah land surface scheme (Chen and Dudhia, 2001), YSU PBL scheme
119 (Hong et al., 2006), and Kain–Fritsch cumulus scheme (Kain., 2004). To improve the
120 meteorological modeling performance, the nudging was performed using the NCEP
121 Automated Data Processing (ADP) data (ds351.0 and ds461.0) and surface observation data
122 from China Meteorological Administration (Zhang et al., 2016). Table S1 summarizes the
123 statistical performance for the meteorological predictions.

124 The anthropogenic emission input was generated based on three emission inventories
125 covering different regions. For the PRD region, a local emission inventory with high
126 resolution for 2010 (Pan et al., 2014) was used. For other regions in China, the emission data
127 for 2013 were from Ma et al. (2017). For other Asian countries, the INTEX-B dataset was
128 used. HONO emissions from transportation sources were calculated based on the HONO/NO_x



129 ratios and NO_x emissions from the transportation sources in the anthropogenic emission
 130 inventory. The HONO/NO_x ratios were set as 0.8% and 2.3% for gasoline and diesel engines,
 131 respectively (Zhang et al., 2016). Natural biogenic emissions were estimated by the Model of
 132 Emissions of Gases and Aerosols from Nature (MEGAN) (Guenther et al., 2006).

133 2.1.2 Parameterization of HONO Sources

134 In addition to the direct anthropogenic emissions, the default CMAQ model has two
 135 HONO more sources, including the gas-phase homogeneous reaction of NO and OH (R7) and
 136 the heterogeneous reactions of NO₂ on surfaces (R8) (Sarwar et al., 2008). The heterogeneous
 137 formation of HONO on the surfaces of particle, urban and leaves was estimated with a
 138 reaction rate $k = 5 \times 10^{-5} \times (S/V)$ as measured by Kurtenbach et al. (2001) under dark
 139 conditions with a relative humidity (RH) of 50%.



142 In the present study, we incorporated four additional HONO sources, as described below.

143 (1) RH-enhancing effects on heterogeneous reaction of NO₂ on surfaces

144 The default heterogeneous reaction rate was based on measurements at a relative
 145 humidity of 50%. However, previous field and lab studies found that surface adsorbed water
 146 played a key role in the heterogeneous conversion and the reaction rate was highly dependent
 147 on the RH level (Finlayson-Pitts et al., 2003; Stutz et al., 2004; Qin et al., 2009). The
 148 laboratory measurements over an RH range of 0% to 80% conducted by Finlayson-Pitts et al.
 149 (2003) showed that the heterogeneous conversion rate increased much faster when RH ≥ 50%
 150 than that when RH < 50%. Based on this result, the RH dependence of the heterogeneous
 151 reaction was considered through scaling the default reaction rate by a factor of f_{RH} in this
 152 study, as shown in the following equation:

$$153 \quad k_{het} = 5 \times 10^{-5} \times f_{RH} \times (S/V) \quad (\text{E1})$$

$$154 \quad f_{RH} = \begin{cases} RH / 50 & (RH < 50) \\ RH / 10 - 4 & (50 \leq RH < 80) \\ 4 & (RH \geq 80) \end{cases}$$



155 (2) Light-enhancing effects on heterogeneous reaction of NO₂ on surfaces

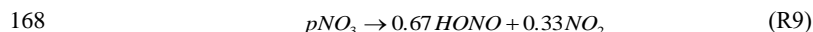
156 The default reaction rate coefficient for the heterogeneous reaction was based on
157 measurements under dark conditions. However, it has been reported that sunlight significantly
158 boosts the heterogeneous generation of HONO (Ndour et al., 2008; Monge et al., 2010;
159 Stemmler et al., 2007). To consider the photo-enhancing effect, we applied a higher reaction
160 rate at daytime (Li et al., 2010; Czader et al., 2012), as shown in the following equation:

$$161 \quad k_{\text{het}} = 1 \times 10^{-3} \times \frac{\text{light intensity}}{400} \times (S/V) \quad (\text{E2})$$

162 where light intensity means the total downward irradiance at the surface, measured in watts per
163 meter squared (W/m²).

164 (3) Photolysis of particulate nitrate in the atmosphere

165 Evidence from recent aircraft observations and laboratory measurements suggested that
166 particulate nitrate in the atmosphere can undergo photolysis to produce HONO and NO₂ (R9)
167 (Ye et al., 2016b, 2017).



169 Ye et al. (2017) reported the photolysis rates ranging from $6.2 \times 10^{-6} \text{ s}^{-1}$ to $5.0 \times 10^{-4} \text{ s}^{-1}$,
170 with a median of $8.3 \times 10^{-5} \text{ s}^{-1}$, at noontime tropical conditions. The reported value was much
171 higher than the photolysis rate of gaseous HNO₃ ($\sim 7 \times 10^{-7} \text{ s}^{-1}$) under the typical tropical
172 noontime conditions (Finlayson-Pitts and Pitts., 2000; Ye et al., 2017). Similar to the
173 methodology of Sarwar et al. (2008), the photolysis rate of particulate nitrate was estimated as
174 the following equation:

$$175 \quad J_{\text{PNO}_3} = \frac{8.3 \times 10^{-5}}{7 \times 10^{-7}} \times J_{\text{HNO}_3\text{-CMAQ}} \quad (\text{E3})$$

176 where $J_{\text{HNO}_3\text{-CMAQ}}$ is the photolysis rate of gaseous HNO₃ calculated online in CMAQ.

177 (4) Photolysis of HNO₃/nitrate deposited on surfaces

178 Field observations and lab studies also indicated that the photolysis of HNO₃/nitrate
179 deposited on the surface could be an important daytime HONO source (R10) (Zhou et al.,
180 2003, 2011; Baergen et al., 2013). Ye et al. (2016a) tested the photolysis of HNO₃/nitrate
181 deposited on various natural and artificial surfaces in the laboratory, and reported the
182 photolysis rates ranging from $6 \times 10^{-6} \text{ s}^{-1}$ to $3.7 \times 10^{-4} \text{ s}^{-1}$, with a median of $3.4 \times 10^{-5} \text{ s}^{-1}$.



$$183 \quad \text{deposited_HNO}_3/\text{nitrate} \rightarrow 0.67\text{HONO} + 0.33\text{NO}_2 \quad (\text{R10})$$

184 This reaction was incorporated into the CMAQ model by assuming deposited
185 HNO₃/nitrate on surfaces to equal the accumulation of dry deposition since the last
186 precipitation event, referring to the method of Sarwar et al. (2008). The photolysis rate of
187 deposited HNO₃/nitrate was estimated as the following equation:

$$188 \quad J_{\text{DNO}_3} = \frac{3.4 \times 10^{-5}}{7 \times 10^{-7}} \times J_{\text{HNO}_3\text{-CMAQ}} \quad (\text{E4})$$

189 2.1.3 Simulation cases

190 Eight simulations were conducted considering different HONO sources, including:

191 **NO_HONO:** without any HONO sources

192 **G:** gas-phase homogeneous reaction (G)

193 **GE:** G + vehicle emissions (E)

194 **GEH (CMAQ-default):** GE + heterogeneous reactions under dark conditions with a RH
195 of 50% (H)

196 **GEHR:** GEH + RH-enhancing effects on heterogeneous reactions (R)

197 **GEHRL:** GEHR + light-enhancing effects on heterogeneous reactions (L)

198 **GEHRLP:** GEHRL + photolysis of particulate nitrate in the atmosphere (P)

199 **GEHRLPD (CMAQ-revised):** GEHRLP + photolysis of HNO₃/nitrate deposited on the
200 surface (D)

201 2.2 Observation data

202 Field observations of HONO and other major air pollutants were conducted at Heshan
203 site (112°55'17"E, 22°42'50"N) in the PRD region (Fig. 1). Hourly HONO concentration was
204 measured using a Long Path Absorption Photometer (LOPAP) (QUMA, Model LOPAP-03)
205 (Heland et al., 2001; Xu et al., 2015). PM_{2.5} concentrations were determined by a Multi Angle
206 Absorption Photometer (Thermo Scientific, Model 5012). Sulfate, nitrate and ammonium in
207 PM_{2.5} were measured by a gas and aerosol collector coupled with an ion chromatography
208 (GAC-IC) system. Gas HNO₃ concentrations were also measured by this GAC-IC system. O₃



209 concentrations were measured by a UV photometric analyzer (Thermo Scientific, Model 49i).
210 NO₂ concentrations were measured using a chemiluminescence instrument (Thermo Scientific,
211 Model 42i) coupled with a photolytic converter (Droplet Measurement Technologies, model
212 BLC) (Xu et al., 2013).

213 Additionally, hourly PM_{2.5}, O₃ and NO₂ observation data at 56 official monitoring sites
214 (Fig.1) in the PRD region were obtained from the Ministry of Environmental Protection
215 (MEP). It should be noted that NO₂ concentrations in the national network were measured
216 using the catalytic conversion method, which overestimates NO₂, especially during the period
217 with active photochemistry and at the location away from the primary emission sources (Xu et
218 al., 2013). The NO₂ observation data were adjusted based on the method of Zhang et al. (2017).

219 **3 Results and Discussion**

220 **3.1 Observed pollution in this winter episode**

221 During 4-8 January 2017, a severe pollution episode was observed in the PRD region. As
222 shown in Fig. S1, the episode average PM_{2.5} concentrations observed at the Heshan site
223 reached 142 µg/m³, which is nearly twice the respective standard of China (75 µg/m³ for daily
224 average PM_{2.5} concentration). The hourly PM_{2.5} concentration peaked at 382 µg/m³, which
225 was among the highest PM_{2.5} concentrations ever reported in the PRD region (Tan et al., 2009;
226 Wang et al., 2012; Yue et al., 2015). O₃ levels were also high, with a peak of ~150ppb. Fig. S2
227 presented the spatial distribution of observed PM_{2.5} and O₃ on the two heaviest polluted days
228 (5 and 6 January) based on the interpolation of the observation data at the 56 official
229 monitoring sites. It can be seen that the whole western PRD region suffered from severe
230 pollution. On 5 January, the highest PM_{2.5} pollution occurred in Foshan city and its
231 surrounding area, with a peak of 448 µg/m³. On 6 January, the pollution expanded to wider
232 areas.

233 **3.2 Evaluation of model performance**

234 Figure 2 compared the simulated HONO mixing ratios by the default CMAQ model



235 (GEH) and the revised CMAQ model (GEHRLPD) with the observations at Heshan site for
236 4-8 January. For the HONO simulation, the default CMAQ significantly underestimated the
237 levels, with a normalized mean bias (NMB) of -71.6%. The maximum underestimation was
238 6ppb in the early morning of 5 January. The simulated HONO levels in the afternoon were
239 lower than 0.1 ppb in the default CMAQ model. By considering the four additional HONO
240 sources, the model performance was improved considerably, with an NMB of -22.5%. The
241 simulated average daytime HONO mixing ratios increased from 0.37 to 1.44 ppb, and the
242 simulated nighttime HONO values increased from 1.10 to 2.63 ppb. The revised model
243 reproduced the HONO diurnal variation. Underestimation was found on the morning of 5-6
244 and 8 January. One possible reason was that some HONO sources were not considered in this
245 study. For example, previous studies have proposed that deposited HONO can be reserved in
246 dew water on the ground or vegetation during the nighttime and re-released when the dew
247 water evaporate in the morning (He et al., 2006). Overestimation was seen at the nighttime of
248 4 and 7 January, which may be related to the uncertainties of emission inventory, and
249 meteorological simulation, etc.

250 The inclusion of the four additional HONO sources also changed the model performance
251 for other air pollutants. As shown in Fig. S1, the O₃ prediction by the default CMAQ model
252 was not satisfactory, especially for the peak value. For example, on 6 January, the observed
253 maximum 1-h and 8-h O₃ mixing ratios at Heshan site reached 147 ppb and 125 ppb,
254 respectively, exceeding the respective standard of China (~93 ppb and 75 ppb for maximum
255 1-h and 8-h O₃ concentrations, respectively). The simulated levels by the default CMAQ
256 model were just 64ppb and 52ppb, respectively, which failed to predict the non-compliance of
257 O₃ for this episode). In contrast, the revised model was better to reproduce the magnitude. For
258 the episode average, the NMB values decreased from -32.9% to 5.5% for the maximum 8-h
259 O₃. Therefore, it is crucial to include these additional HONO sources into air quality models.
260 For NO₂, the revised model could reproduce its temporal variation in general, although
261 underestimation was seen for some peak NO₂ values. This under-prediction could also explain
262 partially the underestimation of HONO peak values. For PM_{2.5}, improvements also can be
263 seen, especially for the peak values. For the sulfate, nitrate and ammonium components in
264 PM_{2.5}, as shown in Fig.S3, the revised model performed well in reproducing their temporal



265 variations, with correlation coefficients (R value) of 0.5, 0.7 and 0.7, respectively. Compared
266 to the default CMAQ model, the NMB values decreased from -29.8% to -10%, -53.8% to
267 -41.2%, and -32.9% to -14.1% for fine particle sulfate, nitrate and ammonium, respectively.
268 Underestimation could be seen for particle nitrate, especially on 5 January. The possible
269 reason was underestimation of the emissions of NH_3 or other alkaline species (e.g. Ca, K, Na),
270 which led to gas HNO_3 not being converted to particle nitrate sufficiently. The model
271 performance for total nitrate ($\text{TNO}_3 = \text{gaseous HNO}_3 + \text{fine particle nitrate}$) was satisfactory,
272 with an NMB of -3.2% and R of 0.8.

273 Regionally, as shown in Table 1, the simulation results of the revised CMAQ model
274 were in better agreement with the observations, with the NMBs decreasing from -33.3% to
275 0.7%, -8.1% to 4.7%, and 20.6% to 9.4% for 8-hour maximum O_3 , hourly average $\text{PM}_{2.5}$ and
276 hourly average NO_2 values, respectively.

277 The above results indicated the satisfactory performance of the revised CMAQ model to
278 simulate HONO and other major pollutants. It could be used to analyze the formation and
279 impact of HONO in this episode.

280 3.3 Contributions of different sources to HONO concentrations

281 Figure 3 presents the contributions of different HONO sources to the HONO mixing
282 ratios at Heshan site. Heterogeneous generation on surfaces (including RH and light effects,
283 H+R+L) was the largest contributor, representing 72% of the average predicted HONO for the
284 whole day. It contributed up to 81% of the average predicted HONO values during the
285 nighttime (18:00 to 6:00) and ~52% during the daytime (7:00 to 17:00). These findings on the
286 dominant contribution from heterogeneous generation were similar to those in the previous
287 modeling studies (Sarwar et al., 2008; Zhang et al., 2016) and field measurements (Li et al.,
288 2012; Wang et al., 2017a). High relative humidity and solar radiation were two important
289 driving factors for the formation of the high HONO concentrations in this pollution episode.
290 During the nighttime and early morning (18:00 to 8:00), RH-enhancing effects on the
291 heterogeneous generation were significant, due to high relative humidity (70% to 90%) (Fig.
292 S4). The heterogeneous generation of HONO had a ~2-fold increase by considering



293 RH-enhancing effects, compared to that under the uniform relative humidity of 50%. From
294 9:00 to the afternoon, light-enhancing effects became important, contributing approximately
295 25% to HONO levels, due to strong radiation with a maximum of ~ 450 W/m² (Fig. S4). In
296 addition to enhancing the heterogeneous generation, the existence of light also increased
297 HONO values through the photolysis of particle nitrate in the atmosphere and total nitrate
298 deposited on the surface. Due to the high total nitrate concentrations in this pollution episode,
299 these two photolysis sources were dominant during noon and afternoon (11:00 to 17:00),
300 contributing 31% and 36% to the HONO levels, respectively. Vehicle emissions contributed
301 approximately 8% of the daily average HONO values. The gas-phase homogeneous reaction
302 was the smallest source, contributing approximately 3% and 7% of the daily and daytime
303 average HONO values, respectively. Our model simulations suggest that the three additional
304 light-dependent sources (L+P+D) could be an important part of missing daytime sources for
305 the present case.

306 **3.4 Impacts of HONO chemistry on HO_x and O₃**

307 The HO_x (OH+HO₂) radical plays a key role in the atmospheric photochemical process.
308 The photolysis of HONO can produce OH radical, and fast reactions exist between OH and
309 HO₂ radical. Therefore, the photolysis of HONO can affect the abundance of HO_x radical.
310 Figure 4 presents the average diurnal OH and HO₂ variations based on the simulations with
311 and without the HONO sources (NO_HONO vs. GEHRLPD). The diurnal pattern and
312 magnitude of the simulated OH and HO₂ mixing ratios in the GEHRLPD case were
313 comparable to the previous observations in the PRD region and other areas (Lu et al., 2012;
314 Mao et al., 2010). Compared to the results of the NO_HONO simulation, the daytime average
315 OH and HO₂ values were increased by 175% and 336%, respectively. The integrated reaction
316 rate (IRR) analysis tool available in CMAQ was utilized to explore the contribution of
317 HONO photolysis to HO_x radical production relative to other HO_x radical sources in the
318 surface layer (~ 0 to 30 m), including the reaction of H₂O with O (1D) which comes from the
319 photolysis of O₃, HCHO photolysis, H₂O₂ photolysis, and the reaction of O₃ with alkenes and
320 biogenic VOCs. As shown in Fig. 5, HONO photolysis was the dominant HO_x source during



321 the daytime at Heshan site. The daytime average contribution of HONO photolysis to HO_x
322 production was approximately 74%, and the contribution during the morning could be above
323 90%. With the increasing of O₃ concentrations from sunrise to afternoon, the contribution of
324 the O₃ photolysis began to increase and reached a peak of 33.4% at 14:00. Compared to the
325 reported results in the previous studies (Czader et al., 2012; Mao et al., 2010; Tham et al.,
326 2016; Xue et al., 2016; Li et al., 2018c), the contribution of HONO photolysis to HO_x was
327 much larger in the present study, mainly due to the high HONO concentrations in this episode.
328 For example, Xue et al. (2016) and Li et al. (2018c) reported daytime average contributions of
329 less than 30% from HONO photolysis at two sites in Hong Kong. Tham et al. (2016) showed
330 a contribution of less than 50% in the morning at a site in the North China Plain. In these
331 cases, the HONO levels were relatively low, with the peak HONO levels ranging among
332 1-3ppb. The high HONO concentrations at Heshan increased the contribution of HONO
333 photolysis to the formation of HO_x in this winter pollution episode.

334 The enhanced HO_x formation due to HONO chemistry could increase O₃ concentrations.
335 As shown in Fig. 6, the simulated daytime average O₃ mixing ratio at Heshan site in the
336 GEHRLPD case was approximately 24 ppb (70%) higher than that in the NO_HONO case,
337 with a peak increase up to 60 ppb. The O₃ enhancement was much higher than the previous
338 simulation results for the summer cases (Sarwar et al., 2008; Li et al., 2010; Zhang et al.,
339 2016). In addition to higher HONO concentrations, another possible reason was that the
340 VOC/NO_x ratio was lower in winter than that in summer, due to less biogenic VOC emissions
341 and more NO_x emission from fuel combustion in winter. For example, Zou et al. (2015)
342 reported VOC/NO_x values higher than 10:1 in summer and about 5:1 for winter based on
343 1-year observation in Guangzhou, which is about 60 km from the Heshan site. The lower
344 VOC/NO_x ratio increased the sensitivity of O₃ concentrations to HO_x changes through
345 reaction 2 to 4. Therefore, the enhancement of O₃ concentrations was more significant (Li et
346 al., 2018b). Figure 7 presents the spatial distribution of simulated surface O₃ concentrations at
347 15:00 LTC in the NO_HONO and GEHRLPD cases. With HONO sources, the increase of
348 regional average O₃ mixing ratio at 15:00 LTC was 34% (~17 ppb). The above results
349 indicated the significant impacts of HONO chemistry on the atmospheric oxidation capacity
350 and O₃ pollution in the PRD region during this heavy winter episode.



351 3.5 Impacts of HONO chemistry on secondary inorganic aerosol formation

352 Secondary inorganic aerosols, including nitrate, sulfate and ammonium, contributed
353 approximately 50% to PM_{2.5} concentrations during this episode (Fig. S5). Among them,
354 nitrate was the dominant component, with peak concentrations reaching ~110 µg/m³, which
355 was much higher than the sulfate and ammonium concentrations. Particle nitrate can be
356 generated through the partition of HNO₃ to particle phase. The major formation pathway of
357 HNO₃ is the oxidation of NO₂ by OH during the daytime (R11). HNO₃ can also be produced
358 via heterogeneous reactions of N₂O₅ on the particle surface at night (R12 to R14). Therefore
359 HONO chemistry can accelerate the formation of nitrate through the enhancement of
360 atmospheric oxidation capacity (HO_x and O₃).



365 Considering the uncertainty of the partition of gaseous HNO₃ to particle nitrate (see
366 section 3.2), we assessed the impact of HONO chemistry on the sum of HNO₃ and fine
367 particle NO₃⁻ (TNO₃). As shown in Fig. 8, the average TNO₃ concentrations at Heshan site
368 increased by about 17 µg/m³ (67%), and the peak enhancement reached 55 µg/m³ at 10 am on
369 January 6, when the observed PM_{2.5} and nitrate concentration was at its respective highest
370 level. Figure 9 presents the distribution of simulated average surface TNO₃ concentrations in
371 the NO_HONO and GEHRLPD case. With HONO sources, the regional average TNO₃
372 concentrations were increased by 8.4 µg/m³ for the entire episode. The absolute enhancement
373 was more significant in the areas with higher aerosol concentrations. The highest increase for
374 TNO₃ was above 25 µg/m³ for the episode average. Meanwhile, the HONO chemistry also
375 accelerated the formation of other secondary inorganic aerosols. Particle sulfate can be
376 generated through the partition of H₂SO₄ to the particle phase. The major formation pathways
377 of H₂SO₄ include the gaseous oxidation of SO₂ by OH, and the aqueous oxidation of S(IV) by
378 O₃, H₂O₂ and other oxidants. The partition of gaseous NH₃ to particle ammonium was based
379 on the H₂SO₄-HNO₃-NH₃ thermodynamic equilibrium. The simulated enhancements of the



380 average sulfate and ammonium concentrations at Heshan site were 32% and 33%,
381 respectively. The above results indicated that the HONO chemistry also aggravated the
382 particulate pollution during this episode.

383 4 Conclusion

384 This study has identified the major contributors to the observed high HONO levels
385 during a severe winter pollution episode and highlighted the importance of HONO chemistry
386 in the combined photochemical and haze pollution in a subtropical region. Including
387 up-to-date HONO sources in the widely used CMAQ model significantly improved its
388 capability in simulating ambient concentrations of HONO and other major pollutants (e.g. O₃
389 and PM_{2.5}). The model simulations suggested a predominant contribution from NO₂
390 heterogeneous reactions enhanced by humidity and solar radiation. The high HONO
391 concentration significantly increased the atmospheric oxidation capacity and the levels of
392 ozone and secondary aerosols, especially total nitrate. Our study highlights the critical need to
393 include/update HONO sources in regional air quality models in order to predict ozone and
394 other secondary pollutants during heavy pollution events in southern China and similar
395 regions.

396 **Acknowledgments.** This work was sponsored by the Hong Kong Research Grants Council
397 (C5022-14G and A-PolyU502/16).



References

- Acker, K., Moller, D., Wieprecht, W., Meixner, F. X., Bohn, B., Gilge, S., Plass-Dulmer, C., and Berresheim, H.: Strong daytime production of OH from HNO₂ at a rural mountain site, *Geophysical Research Letters*, 33, 10.1029/2005gl024643, 2006.
- Alicke, B., Geyer, A., Hofzumahaus, A., Holland, F., Konrad, S., Patz, H. W., Schafer, J., Stutz, J., Volz-Thomas, A., and Platt, U.: OH formation by HONO photolysis during the BERLIOZ experiment, *Journal of Geophysical Research-Atmospheres*, 108, 10.1029/2001jd000579, 2003.
- Appel, K. W., Napelenok, S. L., Foley, K. M., Pye, H. O. T., Hogrefe, C., Luecken, D. J., Bash, J. O., Roselle, S. J., Pleim, J. E., Foroutan, H., Hutzell, W. T., Pouliot, G. A., Sarwar, G., Fahey, K. M., Gantt, B., Gilliam, R. C., Heath, N. K., Kang, D., Mathur, R., Schwede, D. B., Spero, T. L., Wong, D. C., and Young, J. O.: Description and evaluation of the Community Multiscale Air Quality (CMAQ) modeling system version 5.1, *Geoscientific Model Development*, 10, 1703-1732, 10.5194/gmd-10-1703-2017, 2017.
- Baergen, A. M., and Donaldson, D. J.: Photochemical Renoxification of Nitric Acid on Real Urban Grime, *Environmental Science & Technology*, 47, 815-820, 10.1021/es3037862, 2013.
- Bernard, F., Cazaunau, M., Grosselin, B., Zhou, B., Zheng, J., Liang, P., Zhang, Y. J., Ye, X. N., Daele, V., Mu, Y. J., Zhang, R. Y., Chen, J. M., and Mellouki, A.: Measurements of nitrous acid (HONO) in urban area of Shanghai, China, *Environmental Science and Pollution Research*, 23, 5818-5829, 10.1007/s11356-015-5797-4, 2016.
- Cao, J.-J., Shen, Z.-X., Chow, J. C., Watson, J. G., Lee, S.-C., Tie, X.-X., Ho, K.-F., Wang, G.-H., and Han, Y.-M.: Winter and Summer PM_{2.5} Chemical Compositions in Fourteen Chinese Cities, *J. Air Waste Manage. Assoc.*, 62, 1214-1226, 10.1080/10962247.2012.701193, 2012.
- Chan, C. K., and Yao, X.: Air pollution in mega cities in China, *Atmospheric Environment*, 42, 1-42, 10.1016/j.atmosenv.2007.09.003, 2008.
- Chen, F., and Dudhia, J.: Coupling an advanced land surface-hydrology model with the Penn State-NCAR MM5 modeling system. Part I: Model implementation and sensitivity, *Monthly Weather Review*, 129, 569-585, 10.1175/1520-0493(2001)129<0569:caalsh>2.0.co;2, 2001.
- Czader, B. H., Rappengluck, B., Percell, P., Byun, D. W., Ngan, F., and Kim, S.: Modeling nitrous acid and its impact on ozone and hydroxyl radical during the Texas Air Quality Study 2006, *Atmospheric Chemistry and Physics*, 12, 6939-6951, 10.5194/acp-12-6939-2012, 2012.
- Finlayson-Pitts, B. J., and Pitts, J. N., Jr.: *Chemistry of the Upper and Lower Atmosphere: Theory, Experiments, and Applications*, Academic Press, San Diego, CA, 2000.
- Finlayson-Pitts, B. J., Wingen, L. M., Sumner, A. L., Syomin, D., and Ramazan, K. A.: The heterogeneous hydrolysis of NO₂ in laboratory systems and in outdoor and indoor atmospheres: An integrated mechanism, *Physical Chemistry Chemical Physics*, 5, 223-242, 10.1039/b208564j, 2003.
- Goncalves, M., Dabdub, D., Chang, W. L., Jorba, O., and Baldasano, J. M.: Impact of HONO



- sources on the performance of mesoscale air quality models, *Atmospheric Environment*, 54, 168-176, [10.1016/j.atmosenv.2012.02.079](https://doi.org/10.1016/j.atmosenv.2012.02.079), 2012.
- Guenther, A., Karl, T., Harley, P., Wiedinmyer, C., Palmer, P. I., and Geron, C.: Estimates of global terrestrial isoprene emissions using MEGAN (Model of Emissions of Gases and Aerosols from Nature), *Atmospheric Chemistry and Physics*, 6, 3181-3210, [10.5194/acp-6-3181-2006](https://doi.org/10.5194/acp-6-3181-2006), 2006.
- He, Y., Zhou, X. L., Hou, J., Gao, H. L., and Bertman, S. B.: Importance of dew in controlling the air-surface exchange of HONO in rural forested environments, *Geophysical Research Letters*, 33, [10.1029/2005gl024348](https://doi.org/10.1029/2005gl024348), 2006.
- Heland, J., Kleffmann, J., Kurtenbach, R., and Wiesen, P.: A new instrument to measure gaseous nitrous acid (HONO) in the atmosphere, *Environmental Science & Technology*, 35, 3207-3212, [10.1021/es000303t](https://doi.org/10.1021/es000303t), 2001.
- Hong, S. Y., Noh, Y., and Dudhia, J.: A new vertical diffusion package with an explicit treatment of entrainment processes, *Monthly Weather Review*, 134, 2318-2341, [10.1175/mwr3199.1](https://doi.org/10.1175/mwr3199.1), 2006.
- Hou, S., Tong, S., Ge, M., and An, J.: Comparison of atmospheric nitrous acid during severe haze and clean periods in Beijing, China, *Atmospheric Environment*, 124, 199-206, [10.1016/j.atmosenv.2015.06.023](https://doi.org/10.1016/j.atmosenv.2015.06.023), 2016.
- Huang, R. J., Yang, L., Cao, J. J., Wang, Q. Y., Tie, X. X., Ho, K. F., Shen, Z. X., Zhang, R. J., Li, G. H., Zhu, C. S., Zhang, N. N., Dai, W. T., Zhou, J. M., Liu, S. X., Chen, Y., Chen, J., and O'Dowd, C. D.: Concentration and sources of atmospheric nitrous acid (HONO) at an urban site in Western China, *Science of the Total Environment*, 593, 165-172, [10.1016/j.scitotenv.2017.02.166](https://doi.org/10.1016/j.scitotenv.2017.02.166), 2017.
- Kain, J. S.: The Kain-Fritsch convective parameterization: An update, *Journal of Applied Meteorology*, 43, 170-181, [10.1175/1520-0450\(2004\)043<0170:tkcpau>2.0.co;2](https://doi.org/10.1175/1520-0450(2004)043<0170:tkcpau>2.0.co;2), 2004.
- Kleffmann, J., Gavriloaiei, T., Hofzumahaus, A., Holland, F., Koppmann, R., Rupp, L., Schlosser, E., Siese, M., and Wahner, A.: Daytime formation of nitrous acid: A major source of OH radicals in a forest, *Geophysical Research Letters*, 32, [10.1029/2005gl022524](https://doi.org/10.1029/2005gl022524), 2005.
- Kurtenbach, R., Becker, K. H., Gomes, J. A. G., Kleffmann, J., Lorzer, J. C., Spittler, M., Wiesen, P., Ackermann, R., Geyer, A., and Platt, U.: Investigations of emissions and heterogeneous formation of HONO in a road traffic tunnel, *Atmospheric Environment*, 35, 3385-3394, [10.1016/s1352-2310\(01\)00138-8](https://doi.org/10.1016/s1352-2310(01)00138-8), 2001.
- Li, D., Xue, L., Wen, L., Wang, X., Chen, T., Mellouki, A., Chen, J., and Wang, W.: Characteristics and sources of nitrous acid in an urban atmosphere of northern China: Results from 1-yr continuous observations, *Atmospheric Environment*, 182, 296-306, [10.1016/j.atmosenv.2018.03.033](https://doi.org/10.1016/j.atmosenv.2018.03.033), 2018a.
- Li, G., Lei, W., Zavala, M., Volkamer, R., Dusanter, S., Stevens, P., and Molina, L. T.: Impacts of HONO sources on the photochemistry in Mexico City during the MCMA-2006/MILAGO Campaign, *Atmospheric Chemistry and Physics*, 10, 6551-6567, [10.5194/acp-10-6551-2010](https://doi.org/10.5194/acp-10-6551-2010), 2010.
- Li, Q., Zhang, L., Wang, T., Wang, Z., Fu, X., and Zhang, Q.: "New" Reactive Nitrogen Chemistry Reshapes the Relationship of Ozone to Its Precursors, *Environmental Science & Technology*, 52, 2810-2818, [10.1021/acs.est.7b05771](https://doi.org/10.1021/acs.est.7b05771), 2018b.



- Li, X., Brauers, T., Haseler, R., Bohn, B., Fuchs, H., Hofzumahaus, A., Holland, F., Lou, S., Lu, K. D., Rohrer, F., Hu, M., Zeng, L. M., Zhang, Y. H., Garland, R. M., Su, H., Nowak, A., Wiedensohler, A., Takegawa, N., Shao, M., and Wahner, A.: Exploring the atmospheric chemistry of nitrous acid (HONO) at a rural site in Southern China, *Atmospheric Chemistry and Physics*, 12, 1497-1513, [10.5194/acp-12-1497-2012](https://doi.org/10.5194/acp-12-1497-2012), 2012.
- Li, Y., An, J., Min, M., Zhang, W., Wang, F., and Xie, P.: Impacts of HONO sources on the air quality in Beijing, Tianjin and Hebei Province of China, *Atmospheric Environment*, 45, 4735-4744, [10.1016/j.atmosenv.2011.04.086](https://doi.org/10.1016/j.atmosenv.2011.04.086), 2011.
- Li, Z., Xue, L., Yang, X., Zha, Q., Tham, Y. J., Yan, C., Louie, P. K. K., Luk, C. W. Y., Wang, T., and Wang, W.: Oxidizing capacity of the rural atmosphere in Hong Kong, Southern China, *Science of the Total Environment*, 612, 1114-1122, [10.1016/j.scitotenv.2017.08.310](https://doi.org/10.1016/j.scitotenv.2017.08.310), 2018c.
- Liang, Y. T., Zha, Q. Z., Wang, W. H., Cui, L., Lui, K. H., Ho, K. F., Wang, Z., Lee, S. C., and Wang, T.: Revisiting nitrous acid (HONO) emission from on-road vehicles: A tunnel study with a mixed fleet, *J. Air Waste Manage. Assoc.*, 67, 797-805, [10.1080/10962247.2017.1293573](https://doi.org/10.1080/10962247.2017.1293573), 2017.
- Lin, Y. L., Farley, R. D., and Orville, H. D.: BULK PARAMETERIZATION OF THE SNOW FIELD IN A CLOUD MODEL, *Journal of Climate and Applied Meteorology*, 22, 1065-1092, [10.1175/1520-0450\(1983\)022<1065:bpotsf>2.0.co;2](https://doi.org/10.1175/1520-0450(1983)022<1065:bpotsf>2.0.co;2), 1983.
- Lu, K. D., Rohrer, F., Holland, F., Fuchs, H., Bohn, B., Brauers, T., Chang, C. C., Haeseler, R., Hu, M., Kita, K., Kondo, Y., Li, X., Lou, S. R., Nehr, S., Shao, M., Zeng, L. M., Wahner, A., Zhang, Y. H., and Hofzumahaus, A.: Observation and modelling of OH and HO₂ concentrations in the Pearl River Delta 2006: a missing OH source in a VOC rich atmosphere, *Atmospheric Chemistry and Physics*, 12, 1541-1569, [10.5194/acp-12-1541-2012](https://doi.org/10.5194/acp-12-1541-2012), 2012.
- Ma, Q., Cai, S., Wang, S., Zhao, B., Martin, R. V., Brauer, M., Cohen, A., Jiang, J., Zhou, W., Hao, J., Frostad, J., Forouzanfar, M. H., and Burnett, R. T.: Impacts of coal burning on ambient PM_{2.5} pollution in China, *Atmospheric Chemistry and Physics*, 17, 4477-4491, [10.5194/acp-17-4477-2017](https://doi.org/10.5194/acp-17-4477-2017), 2017.
- Mao, J. Q., Ren, X. R., Chen, S. A., Brune, W. H., Chen, Z., Martinez, M., Harder, H., Lefer, B., Rappengluck, B., Flynn, J., and Leuchner, M.: Atmospheric oxidation capacity in the summer of Houston 2006: Comparison with summer measurements in other metropolitan studies, *Atmospheric Environment*, 44, 4107-4115, [10.1016/j.atmosenv.2009.01.013](https://doi.org/10.1016/j.atmosenv.2009.01.013), 2010.
- Meusel, H., Tamm, A., Kuhn, U., Wu, D., Leifke, A. L., Fiedler, S., Ruckteschler, N., Yordanova, P., Lang-Yona, N., Poehlker, M., Lelieveld, J., Hoffmann, T., Poeschl, U., Su, H., Weber, B., and Cheng, Y.: Emission of nitrous acid from soil and biological soil crusts represents an important source of HONO in the remote atmosphere in Cyprus, *Atmospheric Chemistry and Physics*, 18, 799-813, [10.5194/acp-18-799-2018](https://doi.org/10.5194/acp-18-799-2018), 2018.
- Mlawer, E. J., Taubman, S. J., Brown, P. D., Iacono, M. J., and Clough, S. A.: Radiative transfer for inhomogeneous atmospheres: RRTM, a validated correlated-k model for the longwave, *Journal of Geophysical Research-Atmospheres*, 102, 16663-16682, [10.1029/97jd00237](https://doi.org/10.1029/97jd00237), 1997.
- Mlawer, E. J., and Clough, S. A.: Shortwave clear-sky model measurement intercomparison



- using RRTM, Proceedings of the 8 th Atmospheric Radiation Measurement (ARM) Science Team Meeting, Tucson, Arizona, USA, 1998.
- Monge, M. E., D'Anna, B., Mazri, L., Giroir-Fendler, A., Ammann, M., Donaldson, D. J., and George, C.: Light changes the atmospheric reactivity of soot, Proceedings of the National Academy of Sciences of the United States of America, 107, 6605-6609, 10.1073/pnas.0908341107, 2010.
- Ndour, M., D'Anna, B., George, C., Ka, O., Balkanski, Y., Kleffmann, J., Stemmler, K., and Ammann, M.: Photoenhanced uptake of NO₂ on mineral dust: Laboratory experiments and model simulations, Geophysical Research Letters, 35, 10.1029/2007gl032006, 2008.
- Oswald, R., Behrendt, T., Ermel, M., Wu, D., Su, H., Cheng, Y., Breuninger, C., Moravek, A., Mougin, E., Delon, C., Loubet, B., Pommerening-Roser, A., Sorgel, M., Poschl, U., Hoffmann, T., Andreae, M. O., Meixner, F. X., and Trebs, I.: HONO Emissions from Soil Bacteria as a Major Source of Atmospheric Reactive Nitrogen, Science, 341, 1233-1235, 10.1126/science.1242266, 2013.
- Pan, Y. Y., Li, N., Zheng, J. Y., Yin, S. S., Li, C., Yang, J., Zhong, L. J., and Chen, D. H.: Emission inventory and characteristics of anthropogenic air pollutant sources in Guangdong Province Acta Scientiae Circumstantiae 35, 2655-2669, 2014.
- Qin, M., Xie, P. H., Su, H., Gu, J. W., Peng, F. M., Li, S. W., Zeng, L. M., Liu, J. G., Liu, W. Q., and Zhang, Y. H.: An observational study of the HONO-NO₂ coupling at an urban site in Guangzhou City, South China, Atmospheric Environment, 43, 5731-5742, 10.1016/j.atmosenv.2009.08.017, 2009.
- Ren, X. R., Harder, H., Martinez, M., Leshner, R. L., Olinger, A., Simpas, J. B., Brune, W. H., Schwab, J. J., Demerjian, K. L., He, Y., Zhou, X. L., and Gao, H. G.: OH and HO₂ chemistry in the urban atmosphere of New York City, Atmospheric Environment, 37, 3639-3651, 10.1016/s1352-2310(03)00459-x, 2003.
- Sarwar, G., Roselle, S. J., Mathur, R., Appel, W., Dennis, R. L., and Vogel, B.: A comparison of CMAQ HONO predictions with observations from the northeast oxidant and particle study, Atmospheric Environment, 42, 5760-5770, 10.1016/j.atmosenv.2007.12.065, 2008.
- Stemmler, K., Ndour, M., Elshorbany, Y., Kleffmann, J., D'Anna, B., George, C., Bohn, B., and Ammann, M.: Light induced conversion of nitrogen dioxide into nitrous acid on submicron humic acid aerosol, Atmospheric Chemistry and Physics, 7, 4237-4248, 10.5194/acp-7-4237-2007, 2007.
- Stutz, J., Alicke, B., Ackermann, R., Geyer, A., Wang, S. H., White, A. B., Williams, E. J., Spicer, C. W., and Fast, J. D.: Relative humidity dependence of HONO chemistry in urban areas, Journal of Geophysical Research-Atmospheres, 109, 10.1029/2003jd004135, 2004.
- Su, H., Cheng, Y. F., Shao, M., Gao, D. F., Yu, Z. Y., Zeng, L. M., Slanina, J., Zhang, Y. H., and Wiedensohler, A.: Nitrous acid (HONO) and its daytime sources at a rural site during the 2004 PRIDE-PRD experiment in China, Journal of Geophysical Research-Atmospheres, 113, 10.1029/2007jd009060, 2008.
- Su, H., Cheng, Y. F., Oswald, R., Behrendt, T., Trebs, I., Meixner, F. X., Andreae, M. O., Cheng, P., Zhang, Y., and Poschl, U.: Soil Nitrite as a Source of Atmospheric HONO and OH Radicals, Science, 333, 1616-1618, 10.1126/science.1207687, 2011.



- Tan, J. H., Duan, J. C., He, K. B., Ma, Y. L., Duan, F. K., Chen, Y., and Fu, J. M.: Chemical characteristics of PM_{2.5} during a typical haze episode in Guangzhou, *J. Environ. Sci.*, 21, 774-781, 10.1016/s1001-0742(08)62340-2, 2009.
- Tham, Y. J., Wang, Z., Li, Q., Yun, H., Wang, W., Wang, X., Xue, L., Lu, K., Ma, N., Bohn, B., Li, X., Kecorius, S., Groess, J., Shao, M., Wiedensohler, A., Zhang, Y., and Wang, T.: Significant concentrations of nitryl chloride sustained in the morning: investigations of the causes and impacts on ozone production in a polluted region of northern China, *Atmospheric Chemistry and Physics*, 16, 14959-14977, 10.5194/acp-16-14959-2016, 2016.
- Wang, G., Zhang, R., Gomez, M. E., Yang, L., Zamora, M. L., Hu, M., Lin, Y., Peng, J., Guo, S., Meng, J., Li, J., Cheng, C., Hu, T., Ren, Y., Wang, Y., Gao, J., Cao, J., An, Z., Zhou, W., Li, G., Wang, J., Tian, P., Marrero-Ortiz, W., Secrest, J., Du, Z., Zheng, J., Shang, D., Zeng, L., Shao, M., Wang, W., Huang, Y., Wang, Y., Zhu, Y., Li, Y., Hu, J., Pan, B., Cai, L., Cheng, Y., Ji, Y., Zhang, F., Rosenfeld, D., Liss, P. S., Duce, R. A., Kolb, C. E., and Molina, M. J.: Persistent sulfate formation from London Fog to Chinese haze, *Proceedings of the National Academy of Sciences of the United States of America*, 113, 13630-13635, 10.1073/pnas.1616540113, 2016.
- Wang, J., Zhang, X., Guo, J., Wang, Z., and Zhang, M.: Observation of nitrous acid (HONO) in Beijing, China: Seasonal variation, nocturnal formation and daytime budget, *The Science of the total environment*, 10.1016/j.scitotenv.2017.02.159, 2017a.
- Wang, S. S., Zhou, R., Zhao, H., Wang, Z. R., Chen, L. M., and Zhou, B.: Long-term observation of atmospheric nitrous acid (HONO) and its implication to local NO₂ levels in Shanghai, China, *Atmospheric Environment*, 77, 718-724, 10.1016/j.atmosenv.2013.05.071, 2013.
- Wang, T., Lam, K. S., Lee, A. S. Y., Pang, S. W., and Tsui, W. S.: Meteorological and chemical characteristics of the photochemical ozone episodes observed at Cape D'Aguilar in Hong Kong, *Journal of Applied Meteorology*, 37, 1167-1178, 10.1175/1520-0450(1998)037<1167:maccot>2.0.co;2, 1998.
- Wang, T., and Kwok, J. Y. H.: Measurement and analysis of a multiday photochemical smog episode in the Pearl River delta of China, *Journal of Applied Meteorology*, 42, 404-416, 10.1175/1520-0450(2003)042<0404:maoam>2.0.co;2, 2003.
- Wang, T., Xue, L., Brimblecombe, P., Lam, Y. F., Li, L., and Zhang, L.: Ozone pollution in China: A review of concentrations, meteorological influences, chemical precursors, and effects, *Science of the Total Environment*, 575, 1582-1596, 10.1016/j.scitotenv.2016.10.081, 2017b.
- Wang, X. M., Ding, X., Fu, X. X., He, Q. F., Wang, S. Y., Bernard, F., Zhao, X. Y., and Wu, D.: Aerosol scattering coefficients and major chemical compositions of fine particles observed at a rural site hit the central Pearl River Delta, South China, *J. Environ. Sci.*, 24, 72-77, 10.1016/s1001-0742(11)60730-4, 2012.
- Xu, J., Zhang, Y., and Wang, W.: Numerical study on the impacts of heterogeneous reactions on ozone formation in the Beijing urban area, *Advances in Atmospheric Sciences*, 23, 605-614, 10.1007/s00376-006-0605-1, 2006.
- Xu, Z., Wang, T., Xue, L. K., Louie, P. K. K., Luk, C. W. Y., Gao, J., Wang, S. L., Chai, F. H., and Wang, W. X.: Evaluating the uncertainties of thermal catalytic conversion in



- measuring atmospheric nitrogen dioxide at four differently polluted sites in China, *Atmospheric Environment*, 76, 221-226, 10.1016/j.atmosenv.2012.09.043, 2013.
- Xu, Z., Wang, T., Wu, J. Q., Xue, L. K., Chan, J., Zha, Q. Z., Zhou, S. Z., Louie, P. K. K., and Luk, C. W. Y.: Nitrous acid (HONO) in a polluted subtropical atmosphere: Seasonal variability, direct vehicle emissions and heterogeneous production at ground surface, *Atmospheric Environment*, 106, 100-109, 10.1016/j.atmosenv.2015.01.061, 2015.
- Xue, L., Gu, R., Wang, T., Wang, X., Saunders, S., Blake, D., Louie, P. K. K., Luk, C. W. Y., Simpson, I., Xu, Z., Wang, Z., Gao, Y., Lee, S., Mellouki, A., and Wang, W.: Oxidative capacity and radical chemistry in the polluted atmosphere of Hong Kong and Pearl River Delta region: analysis of a severe photochemical smog episode, *Atmospheric Chemistry and Physics*, 16, 9891-9903, 10.5194/acp-16-9891-2016, 2016.
- Xue, L. K., Wang, T., Gao, J., Ding, A. J., Zhou, X. H., Blake, D. R., Wang, X. F., Saunders, S. M., Fan, S. J., Zuo, H. C., Zhang, Q. Z., and Wang, W. X.: Ground-level ozone in four Chinese cities: precursors, regional transport and heterogeneous processes, *Atmospheric Chemistry and Physics*, 14, 13175-13188, 10.5194/acp-14-13175-2014, 2014.
- Ye, C., Gao, H., Zhang, N., and Zhou, X.: Photolysis of Nitric Acid and Nitrate on Natural and Artificial Surfaces, *Environmental Science & Technology*, 50, 3530-3536, 10.1021/acs.est.5b05032, 2016a.
- Ye, C., Zhang, N., Gao, H., and Zhou, X.: Photolysis of Particulate Nitrate as a Source of HONO and NO_x, *Environmental Science & Technology*, 51, 6849-6856, 10.1021/acs.est.7b00387, 2017.
- Ye, C. X., Zhou, X. L., Pu, D., Stutz, J., Festa, J., Spolaor, M., Tsai, C., Cantrell, C., Mauldin, R. L., Campos, T., Weinheimer, A., Hornbrook, R. S., Apel, E. C., Guenther, A., Kaser, L., Yuan, B., Karl, T., Haggerty, J., Hall, S., Ullmann, K., Smith, J. N., Ortega, J., and Knote, C.: Rapid cycling of reactive nitrogen in the marine boundary layer, *Nature*, 532, 489-491, 10.1038/nature17195, 2016b.
- Yue, D. L., Zhong, L. J., Zhang, T., Shen, J., Zhou, Y., Zeng, L. M., Dong, H. B., and Ye, S. Q.: Pollution Properties of Water-Soluble Secondary Inorganic Ions in Atmospheric PM_{2.5} in the Pearl River Delta Region, *Aerosol and Air Quality Research*, 15, 1737-1747, 10.4209/aaqr.2014.12.0333, 2015.
- Yun, H., Wang, Z., Zha, Q., Wang, W., Xue, L., Zhang, L., Li, Q., Cui, L., Lee, S., Poon, S. C. N., and Wang, T.: Nitrous acid in a street canyon environment: Sources and contributions to local oxidation capacity, *Atmospheric Environment*, 167, 223-234, 10.1016/j.atmosenv.2017.08.018, 2017.
- Zhang, L., Wang, T., Zhang, Q., Zheng, J., Xu, Z., and Lv, M.: Potential sources of nitrous acid (HONO) and their impacts on ozone: A WRF-Chem study in a polluted subtropical region, *Journal of Geophysical Research-Atmospheres*, 121, 3645-3662, 10.1002/2015jd024468, 2016.
- Zhang, L., Li, Q. Y., Wang, T., Ahmadov, R., Zhang, Q., Li, M., and Lv, M. Y.: Combined impacts of nitrous acid and nitryl chloride on lower-tropospheric ozone: new module development in WRF-Chem and application to China, *Atmospheric Chemistry and Physics*, 17, 9733-9750, 10.5194/acp-17-9733-2017, 2017.
- Zhang, Q., Streets, D. G., Carmichael, G. R., He, K. B., Huo, H., Kannari, A., Klimont, Z., Park, I. S., Reddy, S., Fu, J. S., Chen, D., Duan, L., Lei, Y., Wang, L. T., and Yao, Z. L.:



- Asian emissions in 2006 for the NASA INTEX-B mission, *Atmospheric Chemistry and Physics*, 9, 5131-5153, 10.5194/acp-9-5131-2009, 2009.
- Zhang, Y. H., Su, H., Zhong, L. J., Cheng, Y. F., Zeng, L. M., Wang, X. S., Xiang, Y. R., Wang, J. L., Gao, D. F., Shao, M., Fan, S. J., and Liu, S. C.: Regional ozone pollution and observation-based approach for analyzing ozone-precursor relationship during the PRIDE-PRD2004 campaign, *Atmospheric Environment*, 42, 6203-6218, 10.1016/j.atmosenv.2008.05.002, 2008.
- Zheng, J., Zhong, L., Wang, T., Louie, P. K. K., and Li, Z.: Ground-level ozone in the Pearl River Delta region: Analysis of data from a recently established regional air quality monitoring network, *Atmospheric Environment*, 44, 814-823, 10.1016/j.atmosenv.2009.11.032, 2010.
- Zhou, X. L., Gao, H. L., He, Y., Huang, G., Bertman, S. B., Civerolo, K., and Schwab, J.: Nitric acid photolysis on surfaces in low-NO_x environments: Significant atmospheric implications, *Geophysical Research Letters*, 30, 10.1029/2003gl018620, 2003.
- Zhou, X. L., Zhang, N., TerAvest, M., Tang, D., Hou, J., Bertman, S., Alaghmand, M., Shepson, P. B., Carroll, M. A., Griffith, S., Dusanter, S., and Stevens, P. S.: Nitric acid photolysis on forest canopy surface as a source for tropospheric nitrous acid, *Nature Geoscience*, 4, 440-443, 10.1038/ngeo1164, 2011.
- Zou, Y., Deng, X. J., Zhu, D., Gong, D. C., Wang, H., Li, F., Tan, H. B., Deng, T., Mai, B. R., Liu, X. T., and Wang, B. G.: Characteristics of 1 year of observational data of VOCs, NO_x and O₃ at a suburban site in Guangzhou, China, *Atmospheric Chemistry and Physics*, 15, 6625-6636, 10.5194/acp-15-6625-2015, 2015.



Tables

Table 1. Model performance of the default and revised CMAQ model for O₃, PM_{2.5} and NO₂ at 56 monitoring sites in the PRD region

		OBS ($\mu\text{g}/\text{m}^3$)	SIM ($\mu\text{g}/\text{m}^3$)	Bias ($\mu\text{g}/\text{m}^3$)	NMB (%)	NME (%)	R
8h_max O ₃	GEH (CMAQ-default)	84.79	56.55	-28.24	-33.3	42.69	0.29
	GEHRLPD (CMAQ-revised)		85.42	0.63	0.74	41.76	0.31
hourly PM _{2.5}	GEH (CMAQ-default)	78.75	72.34	-6.40	-8.13	46.6	0.60
	GEHRLPD (CMAQ-revised)		82.44	3.69	4.68	50.64	0.61
hourly NO ₂	GEH (CMAQ-default)	53.39	64.39	11.00	20.61	49.51	0.64
	GEHRLPD (CMAQ-revised)		58.42	5.03	9.42	43.75	0.67



Figure Captions

Fig.1. Model domains and locations of the monitoring sites. Green star represents Heshan site and red dots represent official monitoring sites in the PRD region from the Ministry Environmental Protection of China

Fig.2. Observed and simulated HONO mixing ratios by the default and revised CMAQ model at Heshan site during 4-8 January 2017.

Fig.3. Average diurnal variations of contributions of different HONO sources to the simulated HONO mixing ratios at Heshan site for 4-8 January 2017. The HONO sources include gas-phase homogeneous reaction of NO and OH (G), vehicle emissions (E), heterogeneous reactions under dark condition with the RH of 50% (H), RH-enhancing effects on heterogeneous reactions (R), light-enhancing effects on heterogeneous reactions (L), photolysis of particulate nitrate in the atmosphere (P) and photolysis of HNO₃/nitrate deposited on the surface (D)

Fig.4. Average diurnal variations of OH and HO₂ mixing ratios simulated in the NO_HONO and GEHRLPD case at Heshan site during 4-8 January 2017.

Fig.5. Average diurnal variations of contributions of different reactions to HO_x generation at Heshan site.

Fig.6. Temporal variation of observed and simulated O₃ mixing ratios in the NO_HONO and GEHRLPD case at Heshan site during 4-8 January 2017.

Fig.7. Spatial distributions of O₃ mixing ratios at 15:00 LTC simulated in the NO_HONO and GEHRLPD case, and their difference for domain 3.

Fig.8. Temporal variation of observed and simulated total nitrate, sulfate, and ammonium concentrations in the NO_HONO and GEHRLPD case at Heshan site during 4-8 January 2017.

Fig.9 Spatial distributions of average TNO₃ concentrations simulated in the NO_HONO and GEHRLPD case, and their difference for domain 3 during 4-8 January 2017.

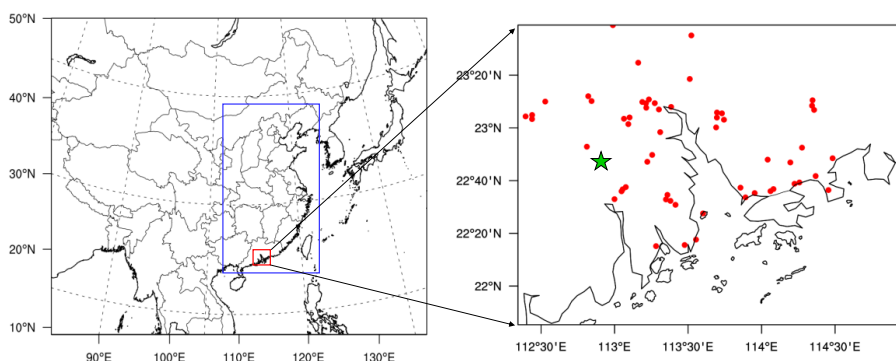


Fig.1. Model domains and locations of the monitoring sites. Green star represents Heshan site and red dots represent official monitoring sites in the PRD region from the Ministry Environmental Protection of China

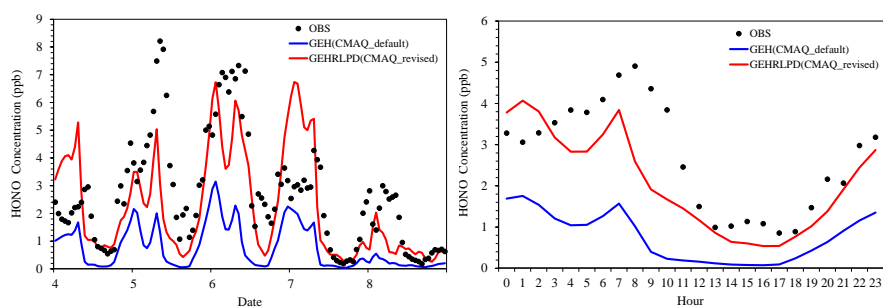


Fig.2. Observed and simulated HONO mixing ratios by the default and revised CMAQ model at Heshan site during 4-8 January 2017.

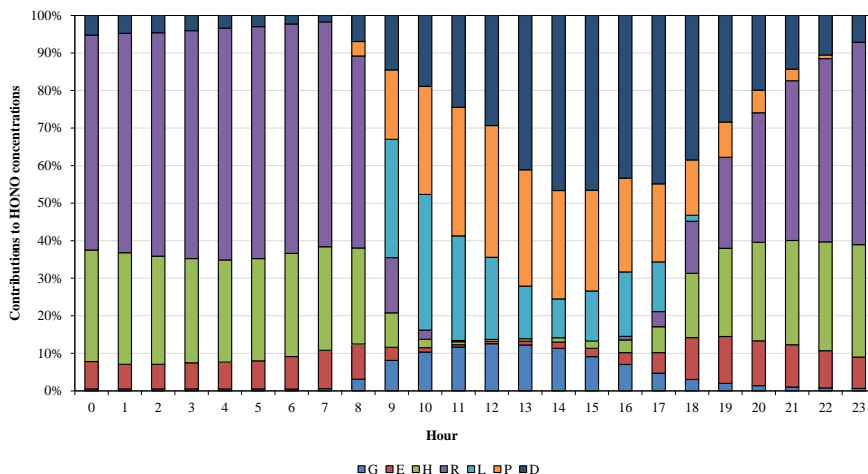


Fig.3. Average diurnal variations of contributions of different HONO sources to the simulated HONO mixing ratios at Heshan site for 4-8 January 2017. The HONO sources include gas-phase homogeneous reaction of NO and OH (G), vehicle emissions (E), heterogeneous reactions under dark condition with the RH of 50% (H), RH-enhancing effects on heterogeneous reactions (R), light-enhancing effects on heterogeneous reactions (L), photolysis of particulate nitrate in the atmosphere (P) and photolysis of HNO₃/nitrate deposited on the surface (D)

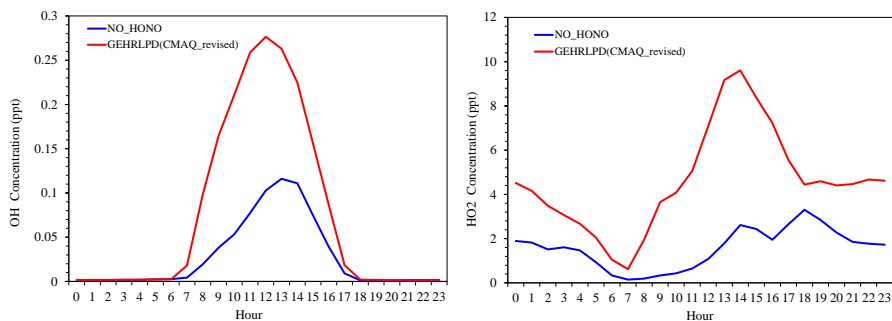


Fig.4. Average diurnal variations of OH and HO₂ mixing ratios simulated in the NO_HONO and GEHRLPD case at Heshan site during 4-8 January 2017.

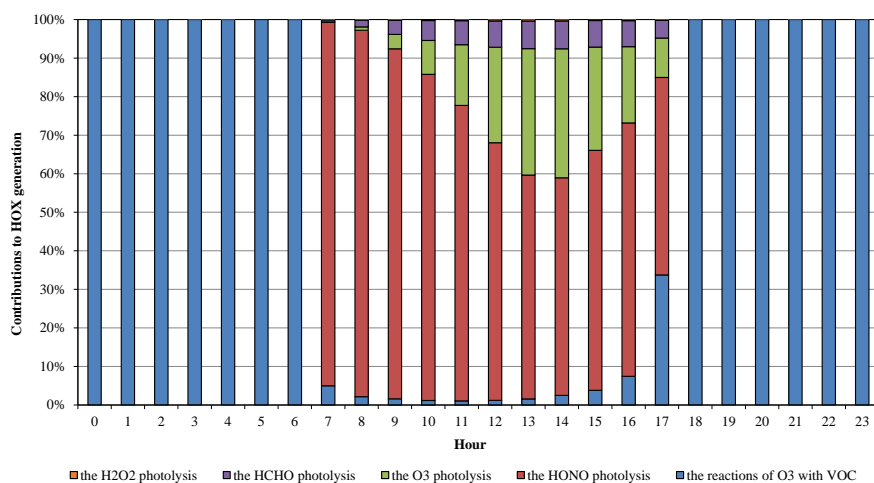


Fig.5. Average diurnal variations of contributions of different reactions to HO_x generation at Heshan site.

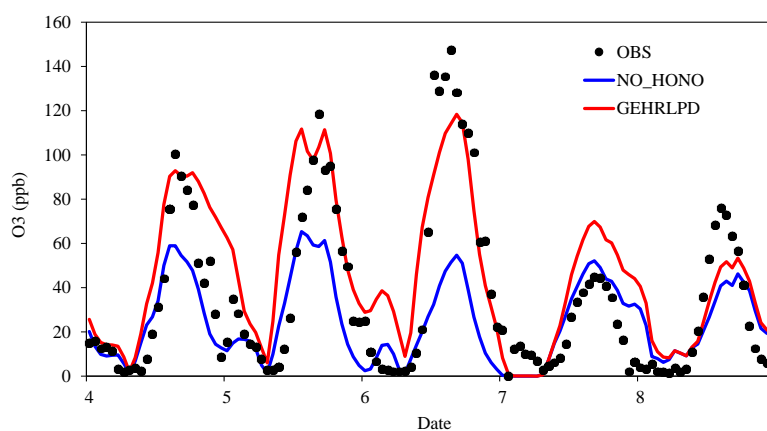


Fig.6. Temporal variation of observed and simulated O₃ mixing ratios in the NO_HONO and GEHRLPD case at Heshan site during 4-8 January 2017.

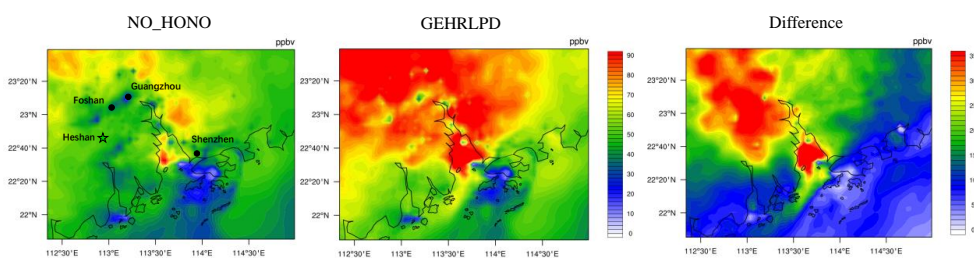


Fig.7. Spatial distributions of O_3 mixing ratios at 15:00 LTC simulated in the NO_HONO and GEHRLPD case, and their difference for domain 3.

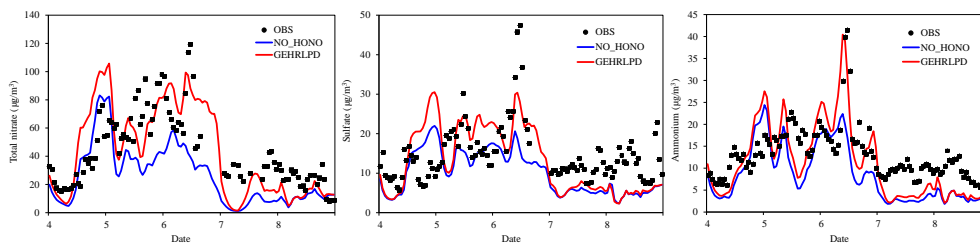


Fig.8. Temporal variation of observed and simulated total nitrate, sulfate, and ammonium concentrations in the NO_HONO and GEHRLPD case at Heshan site during 4-8 January 2017.

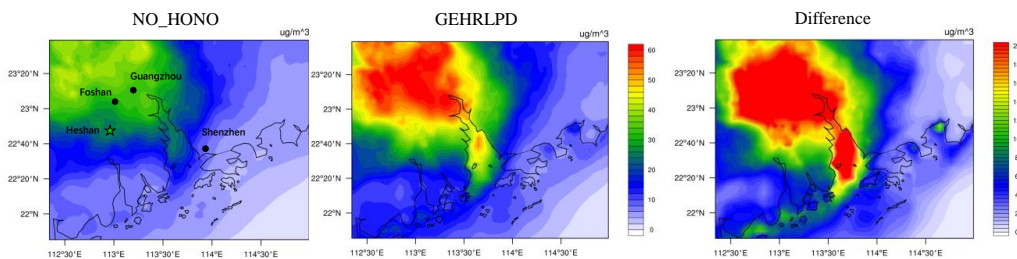


Fig.9 Spatial distributions of average TNO_3 concentrations simulated in the NO_HONO and GEHRLPD case, and their difference for domain 3 during 4-8 January 2017.